Journal of Luminescence 132 (2012) 2330–2340

Contents lists available at SciVerse ScienceDirect

Journal of Luminescence

journal homepage: www.elsevier.com/locate/jlumin

Time-resolved infrared stimulated luminescence signals in feldspars: Analysis based on exponential and stretched exponential functions

V. Pagonis [a,*], P. Morthekai [b,1], A.K. Singhvi [b], J. Thomas [c], V. Balaram [d], G. Kitis [e], R. Chen [f]

[a] McDaniel College, Physics Department, Westminster, MD 21157, USA
[b] Geosciences Division, Physical Research Laboratory, Navrangpura, Ahmedabad 380009, India
[c] Department of Earth Sciences, Pondicherry University, Puducherry 605014, India
[d] National Geophysical Research Institute (CSIR), Uppal Road, Hyderabad 500007, India
[e] Nuclear Physics Laboratory, Aristotle University of Thessaloniki, 54124 Thessaloniki, Greece
[f] Raymond and Beverly Sackler School of Physics and Astronomy, Tel Aviv University, Tel Aviv 69978, Israel

ARTICLE INFO

Article history:
Received 30 November 2011
Received in revised form
11 April 2012
Accepted 16 April 2012
Available online 21 April 2012

Keywords:
Infrared stimulated luminescence (IRSL)
Time-resolved infrared stimulated luminescence (TR-IRSL)
Feldspars
Tunneling
Stretched exponential functions

ABSTRACT

Time-resolved infrared-stimulated luminescence (TR-IRSL) signals from feldspar samples have been the subject of several recent experimental studies. These signals are of importance in the field of luminescence dating, since they exhibit smaller fading effects than the commonly employed continuous-wave infrared signals (CW-IRSL). This paper presents a semi-empirical analysis of TR-IRSL data from feldspar samples, by using a linear combination of exponential and stretched exponential (SE) functions. The best possible estimates of the five parameters in this semi-empirical approach are obtained using five popular commercially available software packages, and by employing a variety of global optimization techniques. The results from all types of software and from the different fitting algorithms were found to be in close agreement with each other, indicating that a global optimum solution has likely been reached during the fitting process. Four complete sets of TR-IRSL data on well-characterized natural feldspars were fitted by using such a linear combination of exponential and SE functions. The dependence of the extracted fitting parameters on the stimulation temperature is discussed within the context of a recently proposed model of luminescence processes in feldspar. Three of the four feldspar samples studied in this paper are K-rich, and these exhibited different behavior at higher stimulation temperatures, than the fourth sample which was a Na-rich feldspar. The new method of analysis proposed in this paper can help isolate mathematically the more thermally stable components, and hence could lead to better dating applications in these materials.

1. Introduction

Time-resolved optically stimulated and infrared stimulated luminescence (TR-OSL and TR-IRSL) time-signals from feldspar samples have been the subject of several recent experimental studies ([1,2] and references therein). These signals are of importance in the field of luminescence dating, since they are believed to exhibit smaller fading effects than the more commonly employed continuous wave infrared stimulated luminescence (CW-IRSL) signals from these materials. Time-resolved experiments provide a simple yet powerful method of separating the various recombination routes in a variety of materials.

One of the common assumptions made during analysis of time resolved luminescence signals from feldspar and quartz is that the observed luminescence decay can be expressed as the sum of several exponential decay functions. Several experimental studies have identified five ranges of lifetimes in these decaying exponentials, namely 30–50 ns, 300–500 ns, 1–2 μs, ~5 μs, and > 10 μs ([3–8]). Some of these lifetimes were interpreted as due to internal transitions within the recombination centers [5]. The assumption that the TR-OSL signal is composed of several decaying exponentials was discussed critically by Ankjærgaard et al. [9], who proposed that it may not be true.

The mathematical expression describing the shape of the TR-OSL and TR-IRSL signals from feldspars is an open research question. In a recent study Jain and Ankjærgaard [1] compared time resolved signals from feldspars under resonant excitation using IR LEDs, as well as under non-resonant excitation using green LED stimulation. Their experiments showed that the use of stimulating light of different wavelengths allows the separation of resonant IR excitation and non-resonant green excitation processes in feldspars. These authors examined the changes occurring in the decay shape of such signals as a function of photon

* Corresponding author. Tel.: +1 410 857 2481; fax: +1 410 386 4624.
E-mail address: vpagonis@mcdaniel.edu (V. Pagonis).
[1] Present address: Institute of Seismological Research, Raisan, Gandhinagar 382009, India.

0022-2313/$ - see front matter © 2012 Elsevier B.V. All rights reserved.
http://dx.doi.org/10.1016/j.jlumin.2012.04.020

energy, storage time after irradiation, and thermal or optical pretreatments of the samples. These experimental results were interpreted within the framework of a model containing several possible recombination routes. Specifically the model includes three possible pathways for charge movement, namely via the ground and excited states of the trap, via the band tail states and through the conduction band. As discussed in detail in Jain and Ankjærgaard [1], the decay form of time resolved signals is most likely not a simple linear sum of exponential decays. In order to analyze their data these authors defined two integral regions termed as the 'Fast signal' and the 'Slow signal', which were defined by integration over different time intervals of the luminescence signals.

This paper presents a new semi-empirical attempt to mathematically characterize the shape of TR-IRSL signals, and to compare the extracted fitting parameters for several different feldspar samples and at a range of stimulation temperatures. A method of analyzing time-resolved experimental data from feldspar is suggested, using a linear combination of an exponential and a stretched exponential (SE) function. These two mathematical components used in the new fitting function are discussed in connection with the above mentioned 'Fast signal' and 'Slow signal' studied by Jain and Ankjærgaard [1].

The advantage of using the well-known stretched exponential functions is that their mathematical properties have been studied extensively, in connection with a variety of relaxation luminescence phenomena (see for example the recent book [10], and references therein). Even though extensive previous theoretical work has shown that relaxation phenomena arising from charge hopping or from tunneling processes can be described mathematically by SE functions, whether SE functions apply to IRSL from feldspar remains to be seen. The OSL decay curve from quartz could presumably also be fitted adequately by an exponential plus a stretched exponential function, but overwhelming experimental evidence has shown that the OSL signal from quartz is, in fact, a linear combination of exponentials.

Although the proposed method of analysis is semi-empirical, the information extracted from the experimental time-resolved curves can provide us with valuable insight in the various relaxation processes taking place in feldspar samples. In this paper we explore the possibility of analyzing these signals on a semi-empirical basis, and also examine the physical implications of analyzing time resolved signals obtained under different stimulation temperatures.

Typical TR-IRSL experimental data for four feldspar samples were fitted accurately, and for a range of stimulation temperatures between 50 and 250 °C. The best possible estimates of the fitting parameters were obtained using five popular commercially available software packages, and by a variety of global optimization techniques. The results from the different software packages and fitting algorithms were in close agreement with each other. The dependence of the extracted fitting parameters on the stimulation temperature is discussed within the context of a recently proposed model of luminescence processes in feldspar [1].

1.1. The stretched exponential (SE) function

Time-resolved luminescence spectroscopy is widely used in the physical, chemical and biological sciences to get information on the structure and dynamics of a variety of luminescent systems. For an extensive list of references pertaining to the SE function and its use to describe luminescence relaxation phenomena, the reader has referred for example to the recent book by Berberan-Santos [10], and the review paper by Chen [11]. In this section we summarize some of the mathematical properties of the SE function, and describe how one can obtain the underlying distribution of decay times, when the luminescence decay law $I(t)$ is known.

Throughout this paper we use the same mathematical notation as in the comprehensive paper by Berberan-Santos et al. [12], unless otherwise indicated. These authors considered the following very general first order phenomenological equation, to describe the luminescence decay law $I(t)$

$$\frac{dI}{dt} = -k(t)I, \tag{1}$$

where $I(t)$ is the luminescence intensity and $k(t)$ represents a time-dependent distribution of decay constants.

In the simplest possible situation, the decay constant $k(t)$ is independent of time, and the solution of Eq. (1) is a simple exponential decay of the form

$$I(t) = I(0)e^{-kt} \tag{2}$$

In cases where an underlying distribution of rate constants $k(t)$ is present, the luminescence decay will no longer be a simple exponential decay as in Eq. (2), but can be represented instead as a general linear combination of single exponentials e^{-kt}, in the following form:

$$I(t) = \int_0^\infty H(k)e^{-kt}dk \tag{3}$$

This relation defines mathematically the function $H(k)$ as the inverse Laplace transform of $I(t)$. From a physical point of view, the function $H(k)$ in Eq. (3) can be understood as *a distribution of amplitudes for the simple exponential decay terms* e^{-kt}.

By rearranging Eq. (1) we obtain

$$k(t)dt = -\frac{dI}{I} \tag{4}$$

Eq. (4) can be integrated formally to yield:

$$I(t) = I(0)\exp\left(-\int_0^t k(u)du\right) = \exp\left(-\int_0^t k(u)du\right), \tag{5}$$

where the decay law $I(t)$ was normalized by setting $I(0)=1$. The parameter u represents a dummy integration variable with the dimensions of time.

The amplitude distribution function $H(k)$ is also normalized, since Eq. (3) with $I(0)=1$, also implies that

$$\int_0^\infty H(k)dk = 1 \tag{6}$$

Berberan-Santos et al. [12] discussed the important topic of extracting the underlying distribution of rate constants $H(k)$ from the experimental luminescence intensity data $I(t)$. They pointed out that this is *an ill-conditioned problem*, since small changes in the experimental decay $I(t)$ can cause arbitrarily large changes in the amplitude distribution function $H(k)$. These authors also point out that it is even possible to fit $I(t)$ accurately with the sum of a few exponential decay terms, even though the physical system possesses an underlying distribution of rate constants. In practice researchers commonly use a mathematical function that can best describe empirically the experimental data. In many cases a Lorentzian or Gaussian continuous distribution function is chosen, to describe the distribution $k(t)$ of the decay rate constants for the physical system under consideration. Berberan-Santos et al. [12] also points out that one can use the SE functions in a complete empirical basis; in such cases the SE fittings provide an indication of the amount of deviation of the luminescence decay law from an exponential behavior.

Berberan-Santos et al. [12] applied the above mathematical formalism to the Kohlrausch decay law, or stretched exponential (SE) function. The Kohlrausch luminescence decay law has the

following mathematical form:

$$I(t) = \exp\left[-(t/\tau_0)^{\beta}\right], \tag{7}$$

where the dimensionless parameter $0<\beta<1$ and τ_0 is the characteristic decay time of the SE, with the dimensions of time. The SE function in Eq. (7) is characterized by two distinct regions; in the initial time region the SE function decays faster than an exponential of lifetime τ_0, while in the second region it decays slower than this exponential. For small values of the parameter β these two time regions have very different behaviors, but as β approaches 1, the two behaviors become very similar. These behaviors are shown in Fig. 1a, while in Fig. 1b the SE functions are compared for different values of the parameter β, with the same decay constant $\tau_0=4$ μs.

A time-dependent rate coefficient $k(t)$ can be calculated by substituting $I(t)$ from Eq. (7) into the general Eq. (4), to obtain

$$k(t) = \frac{\beta}{\tau_0}\left(\frac{t}{\tau_0}\right)^{\beta-1} \tag{8}$$

The inverse of the *decay rate* $k(t)$ is referred to as the *decay time* $\tau=1/k(t)$.

In addition to the distribution of *decay rate constants* $H(k)$ defined above, the same authors also defined a distribution $f(\tau)$ of the *decay time constants* $\tau=1/k(t)$. Such a distribution of time constants $f(\tau)$ can be defined by using an equation similar to Eq. (3), namely

$$I(t) = \int_0^{\infty} f(\tau)e^{-\frac{t}{\tau}}d\tau \tag{9}$$

The two distribution functions $H(k)$ and $f(\tau)$ are complementary, in the sense that they describe the distribution of the decay rate constants $k(t)$, and of the decay time constants $\tau=1/k(t)$ correspondingly. The relationship between the two distribution functions $H(k)$ and $f(\tau)$ is (Berberan-Santos et al., [12], in their Eq. (11))

$$f(\tau) = \frac{1}{\tau^2}H\left(\frac{1}{\tau}\right) \tag{10}$$

As pointed out above, the distribution of rate constants $H(k)$ can be obtained by taking the inverse Laplace transform of the luminescence intensity $I(t)$ as in Eq. (3). In the case of the stretched exponential, it is not possible to obtain $H(k)$ in close analytical form. However, Berberan-Santos et al. [12] presented the following two general equations for obtaining $H(k)$ by numerical integration:

$$H_{\beta}(k) = \frac{\tau_0}{\pi}\int_0^{\infty} \exp(-k\tau_0 u) \times \exp\left[-u^{\beta}\cos(\beta\pi)\right]\sin\left[u^{\beta}\sin(\beta\pi)\right]du \tag{11}$$

and

$$H_{\beta}(k) = \frac{\tau_0}{\pi}\int_0^{\infty} \exp\left[-u^{\beta}\cos\left(\frac{\beta\pi}{2}\right)\right]\cos\left[u^{\beta}\sin\left(\frac{\beta\pi}{2}\right)-k\tau_0 u\right]du \tag{12}$$

Eq. (11) can be used to evaluate numerically the integral for large values of k, while Eq. (12) is easier to integrate numerically and can be used for small values of k. The same authors also presented approximate analytical expressions for $H(k)$. In this paper we use Eqs. (11) and (12) to obtain numerically the distributions functions $H(k)$, for specific values of the parameter β. Examples of the two distributions obtained for $H(k)$ and $f(\tau)$ by using Eqs. (10)–(12) are shown in Fig. 2a and b.

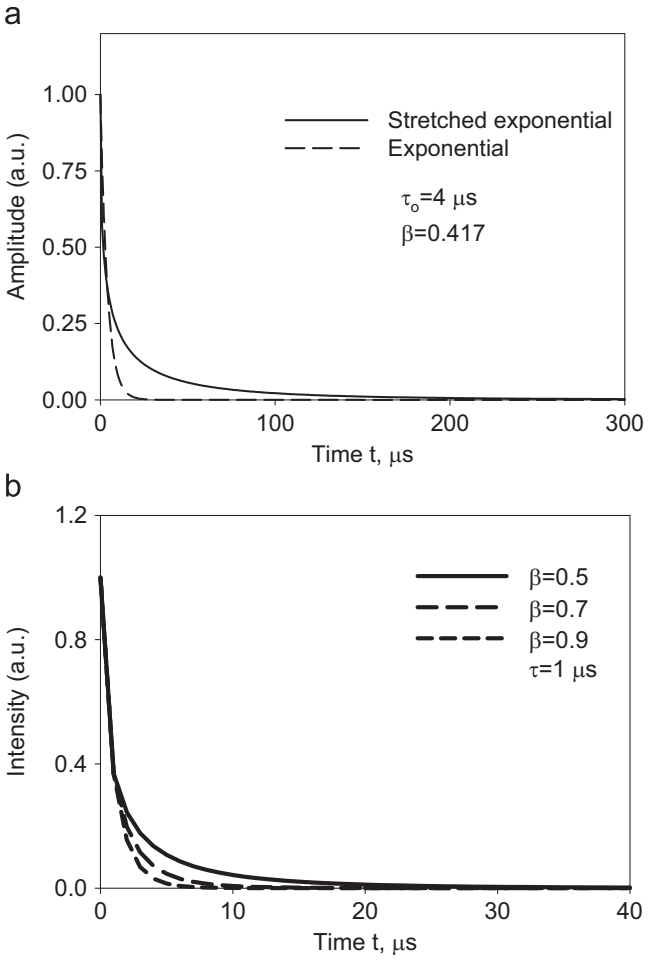

Fig. 1. (a) Comparison of SE and exponential functions for the same time constant $\tau_0=4$ μs. (b) Examples of stretched exponential functions calculated for different values of the parameter β, and for a fixed value of the decay time $\tau_0=1$ μs.

1.2. Sample characteristics and experimental details

Four museum specimens of feldspar samples (FL1, FL2_1, FL2_2 and FL3) were used in this study. X-ray diffraction analysis indicated that the major fractions in FL3 were andesine, and that samples FL1, FL2_1 and FL2_2 were microclines. Diopside was present in all the samples. FL1 additionally contained albite, while FL2_1 contained quartz and oligoclase in smaller proportions (Table 1). Elemental concentrations were estimated using ICP-MS measurements. Assuming that the feldspars contained only K, Na and Ca, the ratios of K:Na:Ca were calculated and these values place FL1, FL2_1 and FL2_2 in the alkali feldspar series. However, sampled FL3 were placed in the plagioclase feldspar series (Table 1). More details about the samples are given in Morthekai et al. [13].

The samples were crushed gently using agate mortar and sieved to obtain the 90–150 μm size fraction, which was used without any further chemical treatment. A few milligrams of samples were mounted on a stainless steel disk using Silkospray silicone oil.

A Risoe TL/OSL Reader DA-20 equipped with pulsing unit and Photon Timer was used for all measurements in this study (Lapp et al., [14] and Bøtter-Jensen et al., [15]). The stimulation was achieved by pulsed IR LEDs (870 ± 40 nm) using ON–OFF time of 50–1000 μs. Total stimulation time was 100 s and hence 95 thousand pulses with a pulse period of 1050 μs were used. The stimulated luminescence emission was detected using a

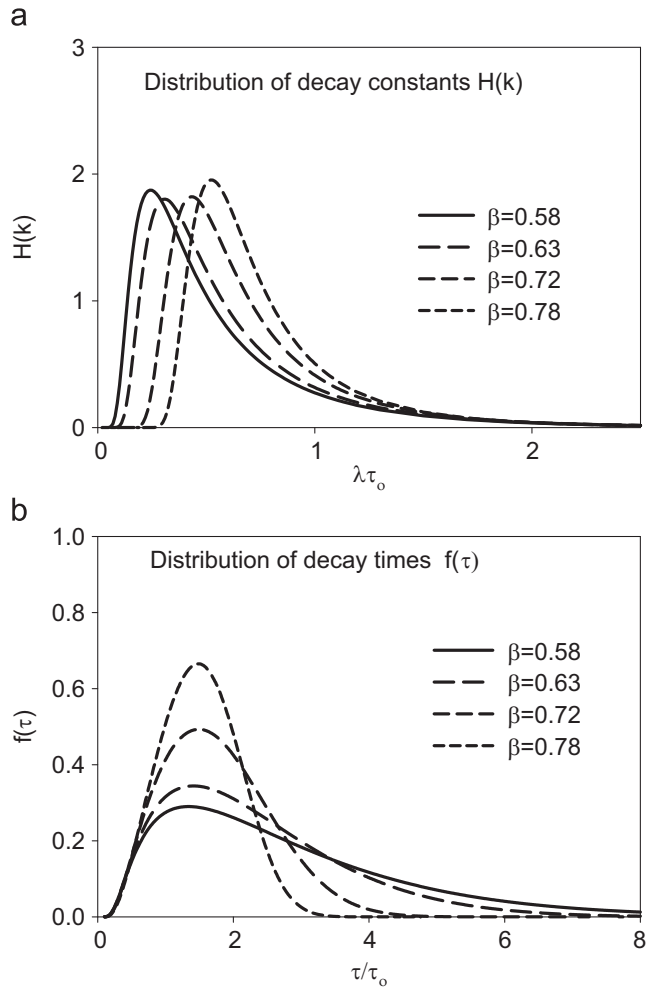

Fig. 2. (a) The distribution function $H(k)$ for the decay time constants $k(t)$, obtained by numerical integration of Eqs. (11) and (12), and for different values of the parameter β. (b) The corresponding distribution function $f(\tau)$ for the decay times τ is calculated using Eq. (10).

Table 1
Sample characteristics.

Sample	Mineral assemblage[a,b]	K:Na:Ca[c] (%)
FL1	Microcline maximum:Albite low:Diopside	67:30:3
FL2_1	Microcline intermediate:Quartz:Oligoclase:Diopside	68:26:6
FL2_2	Microcline intermediate:Diopside	79:15:6
FL3	Andesine:Diopside	3:54:43

[a] Minerals are listed in order of abundance in each sample.
[b] Obtained from XRD analyses.
[c] Obtained from ICP-MS analyses.

photomultiplier tube (EMI 9235QB; 30% QE at ~395 nm) and a combination of optical filters BG-39 (2 mm) and Corning 79–59 (4 mm) were used. These filter combinations transmitted photons in the wavelength region of 395 ± 50 nm. The heating rate was 2 °C/s, and heating was done in nitrogen gas atmosphere.

Complete sets of data were obtained at stimulation temperatures varying from 50 °C to 250 °C, at an interval of 25 °C. All the samples were given an initial dose of 61.8 Gy, except FL2_2 sample which was given a dose of 12.4 Gy. The samples were preheated to 280 °C for 60 s, before measuring the TR-IRSL signals at the variable stimulation temperature (the preheat temperature was 240 °C for sample FL3). After every TR-IRSL measurement and before measuring the signal at a higher stimulation temperature, the remnant luminescence signals were removed by illuminating the sample with IR, while the samples were held for 200 s at 250 °C. Furthermore, after every TR-IRSL and this combined thermal and optical treatment, a TL measurement upto 450 °C was made to monitor for changes in the TL glow curve shape. No changes in shape were observed. The data were normalized by the intensity at the end of ON time (50 μs) and, only the OFF time data were used for further analyses.

1.3. Analysis of TR-IRSL experimental data

In this paper we propose a new method of fitting TR-IRSL data on a semi-empirical basis, by using a linear combination of an exponential decay and a stretched exponential function. The alternative possibility of fitting this experimental data with the sum of three exponential decay functions is discussed later in this paper.

Fig. 3 shows typical TR-IRSL experimental data from Jain and Ankjaergaard ([1], in their Fig. 7a). An aliquot of orthoclase feldspar was given a dose of 25 Gy followed by a preheat temperature of 260 °C for 60 s, and the TR-IRSL signal was measured at 50 °C. The solid line represents the least squares fit with an equation of the

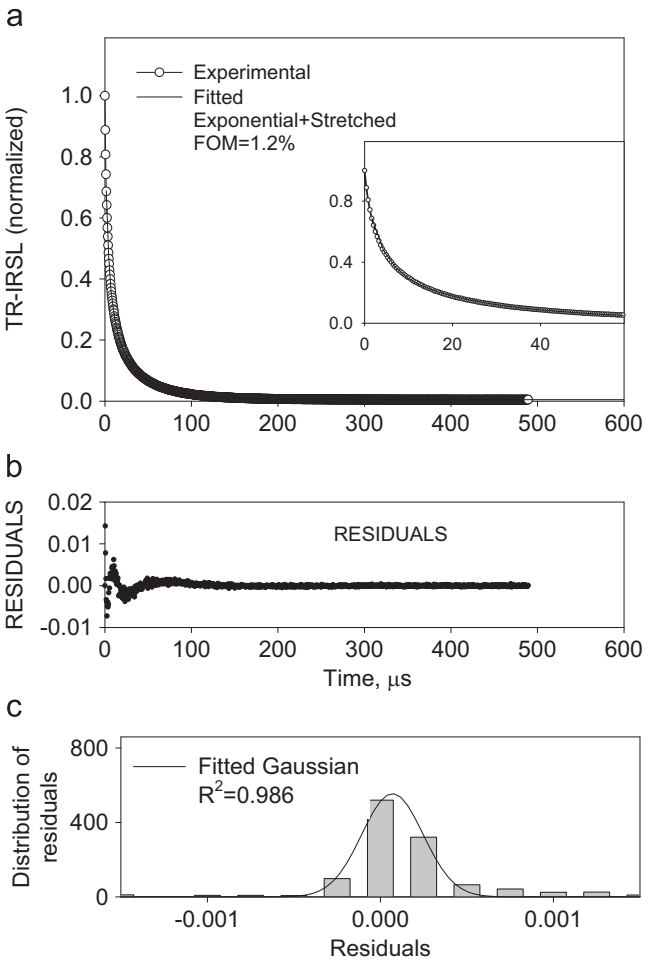

Fig. 3. (a)Time-resolved experimental data from Jain and Ankjærgaard [1], their Fig. 7a, for an aliquot of orthoclase feldspar. The aliquot was given a dose of 25 Gy followed by a preheat temperature of 300 °C for 60 s, and measured at 50 °C. The curve has been normalized to the first experimental point of the TR-IRSL off-time curves, and is fitted with a linear combination of exponential and stretched exponential functions as shown in Eq. (13). The inset shows the first 60 μs of the same data. (b) Residuals (difference between experimental and fitted values) as function of time. (c) Distribution of the residuals for the fitted data in (a).

form:

$$I(t) = A_1 \exp[-t/\tau_1] + A_0 \exp[(-t/\tau_0)^{\beta}] + bgd \quad (13)$$

where the first term is characterized by a single exponential decay time τ_1 and an amplitude A_1, while the second term is characterized by the two parameters τ_0 and β of the stretched exponential function with a corresponding amplitude A_0. The goal of this paper is to obtain the best possible estimates of the six parameters appearing in Eq. (13), and to interpret the fitting values and trends in terms of the most recent and most comprehensive feldspar model. Furthermore, we compare the results from the best fitting procedures used in five popular commercially available software packages.

The data shown in Fig. 3 has been normalized to the first experimental point, and contains a total of 2000 experimental data points. The normalization of the experimental data imposes an additional restriction on the three amplitude parameter amplitudes A_1, A_0 and bgd; these parameters cannot be considered independent of each other, but rather they have to satisfy the relationship:

$$I(0) = A_1 + A_0 + bgd = 1 \quad (14)$$

By substituting the value of A_1 from Eq. (14) into Eq. (13), we arrive at the following equation:

$$I(t) = A_1 \exp[-t/\tau_1] + (1 - A_1 - bgd)\exp[-(t/\tau_0)^{\beta}] + bgd \quad (15)$$

This is the equation used to fit the experimental data in Fig. 3, and it contains five independent fitting parameters τ_1, τ_0, A_1, β and bgd. Since the two amplitudes A_1 and bgd are assumed to be positive, their values in Eq. (15) are restricted between 0 and 1. During the fitting procedures, the values of the two decay constants τ_0 and τ_1 are allowed to vary within the very broad limits of 1 μs and 40 μs. The value of the stretched exponential parameter β is allowed to vary between 0 and 1. These are the only numerical restrictions placed on the parameters during the fitting procedures, unless otherwise indicated in the results section of this paper. Next we provide an overview of the software packages and optimization algorithms used to fit the experimental data.

1.4. Global optimization algorithms in Mathematica, MATLAB, MINUIT, Sigmaplot and ORIGIN

We have carried out numerical and statistical analysis of the data by using several different software packages and a variety of optimization methods. Global optimization algorithms attempt to find the *global optimum*, typically by allowing decrease as well as increase of an objective or merit function. This function is typically a combination of the objective and constraints. Such algorithms are usually computationally more demanding than *local* optimization methods. It is noted that in general, finding a global optimum can be arbitrarily difficult, even without constraints, and so any of the commonly used best fit methods may fail. The software manuals for the packages used here indicate that it may frequently be useful to optimize the function several times, with different starting conditions, and to take the best of the results produced in this manner.

Firstly, we use the composite fitting routines in the program *MINUIT* [16]. Specifically this software uses a sequence of two fitting routines, termed SIMPLEX and MIGRAD. The SIMPLEX method is a multidimensional minimization routine which does not use first derivatives and is usually much slower than MIGRAD. MIGRAD is the best minimizer available within *MINUIT*. It is a variable metric method with inexact line search. Its main weakness is that it depends heavily on knowledge of the first derivatives of the data, and fails miserably if they are very inaccurate.

Secondly, we use several numerical global optimization fitting routines within the commercially available software *Mathematica* as follows. *Mathematica* uses the numeric global optimization routine *NMinimize*, which includes the following nonlinear optimization methods: Nelder–Mead, *differential evolution*, *simulated annealing* and *random search*. These techniques are examples of direct search methods, which tend to converge more slowly, but can be more tolerant to the presence of noise in the function and constraints. The global optimization routines in *Mathematica* are supposed to be flexible enough to avoid being trapped by local optima. In order for *NMinimize* to work, it needs a rectangular initial region to start. This is similar to other numerical methods, in which the users provide a starting point for the fitting procedures. The initial region is specified by giving each variable a finite upper and lower bound. We now describe briefly the four algorithms used within the *Nminimize* command in *Mathematica*.

The Nelder–Mead method is a direct search method. For a function of n variables, the algorithm constucts a "polytope" in n-dimensional space. The fitting process is assumed to have converged if the difference between the best function values in successive polytopes and successive best points, are less than the tolerances provided by the parameters AccuracyGoal and PrecisionGoal. The values of these goal parameters can be set by the user. The Nelder–Mead method tends to work reasonably well for problems that do not have many local minima.

Differential evolution or *genetic algorithm* is a stochastic optimization method, which is based on the principle of biological evolution. This technique starts with a population of parameter sets randomly generated in a defined search space, and the optimum is searched by applying a numerical evolution mechanism. The advantage of this type of algorithm is that it works on a whole population of possible solutions, thus improving the probability of finding the global optimum. As the evolution progresses during these algorithms, it leads to a gradually improved population of individuals, while the mechanisms of selection, crossover and mutation are involved in the creation of new generations. The genetic process is assumed to have converged if the difference between the best function values in the new and old populations, as well as the distance between the new best point and the old best point, are less than the tolerances provided by the user. The *differential evolution* method is computationally expensive, but is relatively robust and tends to work well for problems that have more local minima. Such techniques have been used in quartz luminescence modeling by Adamiec et al. [17,18]. Bluszcz and Adamiec [19] also used this type of *differential evolution* algorithm in carrying out a deconvolution of OSL decay curves into first-order components.

The *random search* algorithm works by generating a population of random starting points and uses a local optimization method from each of the starting points, in order to converge to a local minimum. The best local minimum is chosen to be the solution. Convergence for *random search* is determined by the convergence of the local method for each starting point.

Simulated annealing is also a simple stochastic function minimizer. It is motivated from the physical process of annealing, where a solid is heated to a high temperature and allowed to cool slowly. The physical process allows the atomic structure of the metal to settle to a lower energy state, thus becoming a tougher metal. Using optimization terminology, annealing allows the structure to escape from a local minimum, and to explore and settle on a better, and hopefully a global minimum. Like the *random search* method, *simulated annealing* uses multiple starting points, and finds an optimum starting from each of them. For each starting point, this process is repeated until the maximum number of iterations are reached, the method converges to a point, or the method stays at the same point consecutively for the number of iterations specified by the user.

Thirdly, we use the commercially available software *Sigmaplot*. This software employs a Levenberg–Marquardt type of least squares procedure, to find the best fit parameters.

Next, we used the Levenberg–Marquardt least squares algorithm in the popular software *MATLAB* to fit the experimental data. We also implement and use a two-step optimization algorithm in *MATLAB*, which consists of a first step using simulated annealing algorithm, followed by a least squares minimization technique.

Finally, the commercially available software package *ORIGIN* is used with the option of the Levenberg–Marquardt algorithm to minimize the chi-squared value. Several combinations of starting values for the fitting parameters were tested in this algorithm, and all combinations gave the same results, with one notable exception which is discussed in the Results section of this paper.

2. Results

A comparison of the results from the best fitting procedures used in the five software packages is given in Table 2. The results from several algorithms used in the software package *Mathematica* were identical, upto the fourth significant figure. Specifically the Levenberg–Marquardt, Nelder–Mead, *random search* and *simulated annealing* gave identical results. As mentioned previously, the values of the two amplitudes A_1 and *bgd* in Eq. (15) are restricted between 0 and 1, while the values of the two decay constants τ_0 and τ_1 are allowed to vary within the very broad limits of 1 μs and 40 μs. The value of the stretched exponential parameter β is allowed to vary between 0 and 1. In a few cases the *differential evolution* and the Nelder–Mead algorithms would converge to a local instead of a global optimum solution; in such situations, restricting the range of the allowed parameter values was sufficient to produce a new solution, consistent with the rest of the algorithms in *Mathematica*.

Fig. 4 shows an example of the results of the intermediate steps taken by the *NMinimize* command in *Mathematica*. Specifically this figure shows the effect of using different starting points (τ_1,τ_0) in the best fitting routines. Three different pathways are shown for the optimization procedure, with the starting values $(\tau_1,\tau_0)=(1,1)$, (10,30) and (10,10) μs, in all the three cases, the global optimum solution is reached at (τ_1,τ_0) =(3.00, 11.36) μs, even though it is reached via very different pathways. The starting values for the amplitudes A_1 and *bgd* are taken as 0.3 and 0.01 correspondingly, and the starting value of β was taken in the middle of the interval, $\beta=0.5$.

The goodness of fit was tested by the Figure of Merit (FOM) by Balian and Eddy [20] which can be expressed as

$$FOM = \sum \frac{|Y_{Expt} - Y_{Fit}|}{A}, \quad (16)$$

where Y_{Exp} is the experimental set of data, Y_{Fit} is the fitted curve, and A is the area of the fitted curve. The Figure of Merit (FOM) for the fitted data in Fig. 3 was FOM=012=1.2%, from all software packages and algorithms used in this paper. In general, a FOM value around 1% is considered an excellent fit for experimental data. Also Fig. 3b shows the residuals, representing the difference between the experimental data Y_{Exp} and the corresponding best fit values Y_{Fit}. The values of the residuals are less than 1.5% of the corresponding experimental values Y_{Exp}, for all data points. In Fig. 3c the distribution of the residuals is shown, fitted to a Gaussian function; the good fit indicates that the residuals can be considered a reasonable approximation to white noise.

Fig. 5 shows an alternative fit to the same experimental data, using the linear combination of three exponential functions. The result of the fits is excellent, with the residuals being smaller than 0.4% of the experimental values, at all data points. The FOM value of this fit is 1.4%.

The results from the *MINUIT* optimization procedures were very close to all the algorithms used in *Mathematica*. The difference between the two packages were of the order of 1% in all parameters, except in the case of parameter t_1 which varies by ~4% between these two software packages.

The Levenberg–Marquardt algorithms in *Sigmaplot*, *ORIGIN* and in *MATLAB* produced identical results with the optimization techniques in *Mathematica*. It is worth mentioning here a specific case involving *ORIGIN* software. When the initial values of τ_1, τ_0 and β were chosen as 39 μs, 39 μs, and 0.9 then another minimum was found with a mathematically satisfactory fit. Furthermore, if the starting value of β was chosen as $\beta=0.1$ in the same example, then the "correct" value of the fitting parameters were recovered. This example serves as a warning that initial values far from the "correct" values may give a false result.

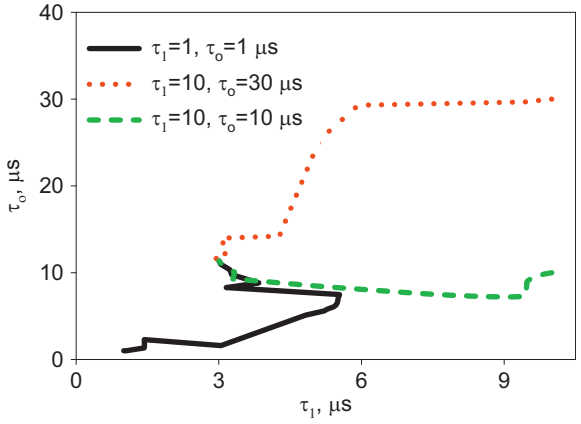

Fig. 4. Example of the results from intermediate steps taken by the *NMinimize* command in *Mathematica*, using different starting points (τ_0,τ_1) in the best fitting routines. Three different pathways are shown for the optimization procedure, with the starting values $(\tau_1,\tau_0)=(1,1)$, (10,30) and (10,10) μs; in all the three cases, the global optimum solution is reached at $(\tau_1,\tau_0)=(3.00, 11.36)$ μs, even though it is reached via very different pathways. The initial values of the other parameters were kept constant with $A_1=0.3$. $bgd=0.01$ and $\beta=0.5$.

Table 2
A comparison of the results from the best fitting procedures used in the four software packages, as discussed in the text. In the case of Mathematica four different algorithms are used: *genetic algorithm*, *simulated annealing*, Levenberg–Marqardt, Nelder–Mead and *random search*.

Parameter	*MINUIT*	*Sigmaplot*	*Mathematica*	*MATLAB*	*MATLAB*	*ORIGIN*
	(2-stage algorithm)	(Levenberg–Marqardt)	(4 algorithms)	(2-stage algorithm)	(Levenberg–Marqardt)	(Levenberg–Marqardt)
A_1	0.299	0.289	0.289	0.280	0.289	0.289
τ_1	3.127	3.002	3.002	2.960	3.002	3.002
τ_0	11.52	11.35	11.35	10.93	11.35	11.35
β	0.603	0.602	0.602	0.594	0.602	0.602
bgd	0.00439	0.00440	0.00448	0.00436	0.0048	0.00448

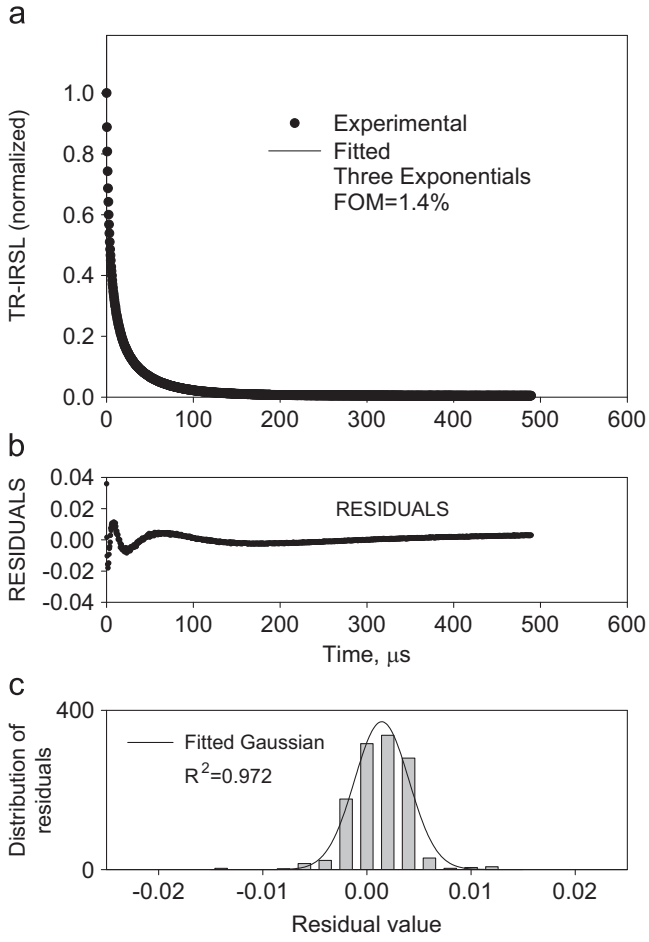

Fig. 5. TR-IRSL experimental data fitted using three exponential components (a) Residuals (difference between experimental and fitted values) as function of time and (b) distribution of the residuals for the fitted data in (a).

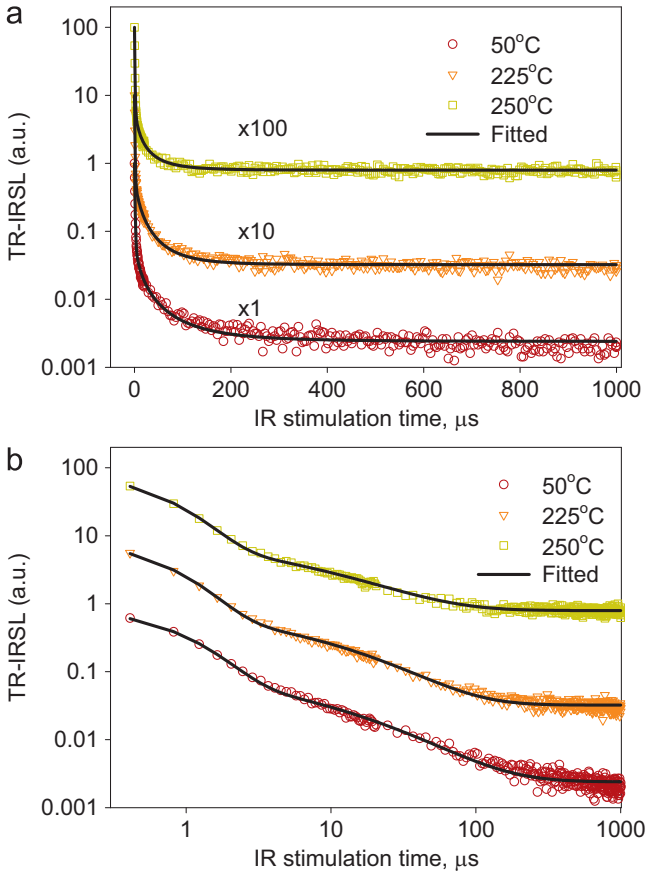

Fig. 6. (a) Typical results of fitting three sets of experimental TR-IRSL data at different stimulation temperatures in the range 50–250 °C, for Na-rich sample FL3. (b) The same data is shown on a log-log scale. The data shown were normalized to the first experimental point, and each curve contains a total of 2,441 experimental data points, measured every 0.4096 μs. For clarity, only every tenth experimental point is shown in Fig. 6a and b for times $t > 20$ μs. The three experimental curves were multiplied by the scaling factors shown, in order to show more clearly the differences between them. The solid lines represent the least squares fits using Eq. (15).

However, if one uses several different algorithms based on completely different search methods, one can have increased confidence that a true global minimum may have been reached.

In some cases, the software packages and algorithms tend to converge to local instead of global optimum solutions; this is a well known problem, inherent in all fitting procedures of this type. However, the fact that several different types of software packages as well as several diverse numerical algorithms in Table 2 converge towards the *same* best set of fitting parameters, provides us with confidence that a global optimum solution very likely has been reached during the fitting procedure.

3. New experimental data for feldspar samples

Fig. 6a shows typical TR-IRSL experimental data for stimulation temperatures of 50, 225 and 250 °C. Fig. 6b shows the same data on a log–log scale. The data shown was normalized to the first experimental point, and each curve contained a total of 2441 experimental data points, measured every 0.4096 μs. For clarity, only every tenth experimental point is shown in Fig. 6a and b for times $t > 20$ μs. Furthermore, the three experimental curves were multiplied by the scaling factors shown, in order to show more clearly the differences between them. The solid lines in Fig. 6a and b represent the least squares fits to the data using Eq. (15). In all fitted data presented in this paper, the FOM values ranged from 0.3% to 4%, indicating that the semi-empirical function (15) can successfully represent time resolved signals in feldspars.

Fig. 7 shows the parameters extracted from the experimental data in Fig. 6, at different stimulation temperatures in the range of 50–250 °C, and for all 4 feldspar samples studied. Specifically, Fig. 7a shows the time constant τ_1 characterizing the single exponential function in Eq. (15), as a function of the stimulation temperature. Similarly, Fig. 7b and c shows the corresponding fitting parameters τ_0, β for the stretched exponential function.

Fig. 7a shows that as the stimulation temperature is increased, the decay time τ_1 characterizing the single exponential function for samples FL1, FL2_1 and FL2_2 gradually decreases from a value of ~2 μs at 50 °C, to a smaller value of ~1.5 μs at the highest stimulation temperature of 250 °C. Sample FL3 shows a similar overall behavior, with a smaller decay time τ_1 gradually decreasing from a value of ~0.8 μs at 50 °C, to a value of ~0.6 μs at a stimulation temperature of 250 °C. This different behavior of sample FL3 can possibly be attributed to the fact that it is a Na-rich sample, while the other three samples are K-rich feldspars.

Fig. 7b shows that as the stimulation temperature is increased, the decay time τ_0 characterizing the stretched exponential function for samples FL2_1 and FL2_2 gradually decreases from a value of ~10 μs at 50 °C, to a smaller value of ~8 μs at a stimulation temperature of 250 °C. Samples FL1 and FL3 show a different behavior, namely an initial increase of the decay time τ_0 for temperatures upto ~150 °C, followed by a gradual decrease at the higher stimulation temperatures.

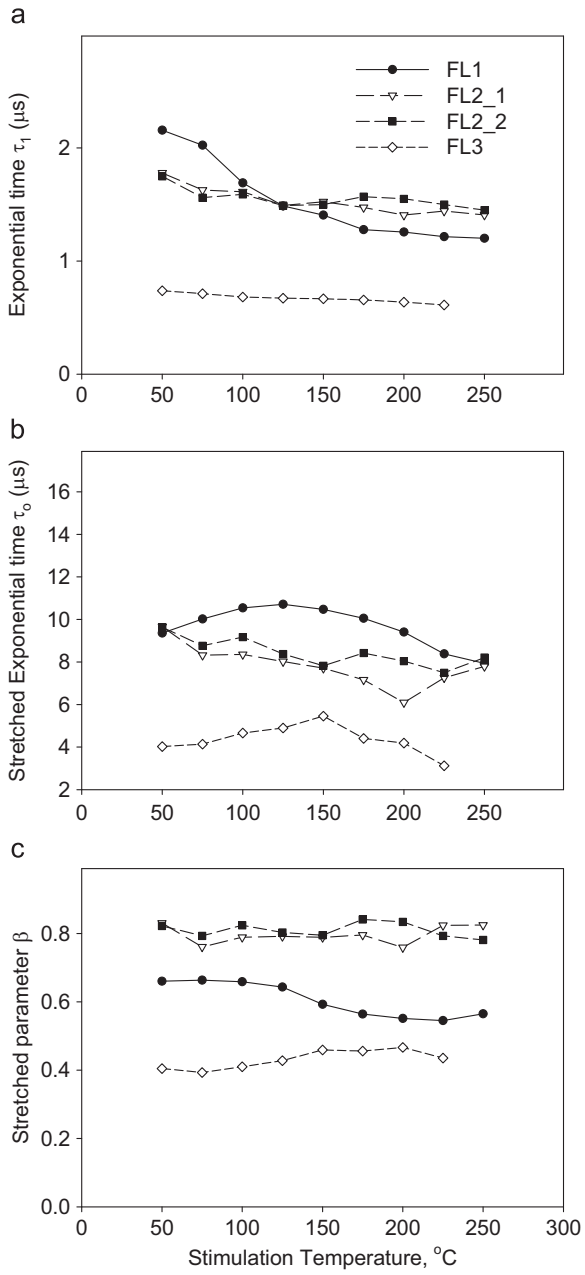

Fig. 7. The parameters extracted from the experimental data in Fig. 6, at different stimulation temperatures in the range 50–250 °C, and for all four feldspar samples studied. (a) The time constant τ_1 characterizing the single exponential function in Eq. (15) (b) and (c) The corresponding fitting parameters τ_0, β for the stretched exponential function. Na-rich sample FL3 shows a different behavior from the three other samples which are K-rich feldspars.

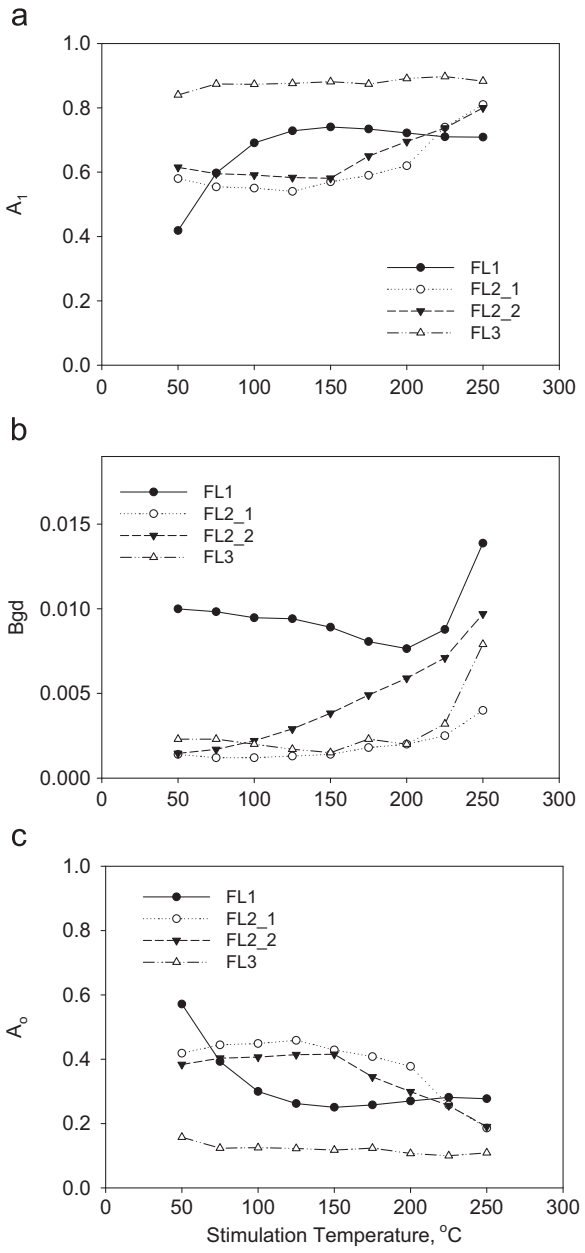

Fig. 8. The amplitude A_1 characterizing the exponential function in the fitting Eq. (15), at the various stimulation temperatures. (a) The background parameter *bgd* at the various stimulation temperatures. (b)The amplitude A_0 characterizing the stretched exponential function, at the various stimulation temperatures.

Fig. 7c shows the corresponding stretched exponential parameter β, at the various stimulation temperatures. It is seen that for samples FL2_1 and FL2_2 this parameter remains practically constant at a value of $\beta \sim 0.80 \pm 0.01$. Sample FL1 shows a different behavior, namely a constant value of $\beta \sim 0.66$ upto a stimulation temperature of 100 °C, followed by a gradual decrease of this parameter to $\beta \sim 0.55$ at the higher stimulation temperatures. The Na-rich sample FL3 once more shows a different behavior than the K-rich samples, namely a small gradual increase from a value of $\beta \sim 0.40$ to a value of $\beta \sim 0.47$ at the higher stimulation temperatures.

Fig. 8a shows the amplitude A_1 characterizing the exponential function, at the various stimulation temperatures. It is seen that the Na-rich sample FL3 once more shows a different behavior than the three K-rich feldspars, with its value remaining practically constant at $A_1 \sim 0.90$ for all stimulation temperatures. This means that ~90% of the initial TR-IRSL signal at time $t=0$, is due to the exponential component for all stimulation temperatures. Samples FL2_1 and FL2_2 show a similar behavior to each other, with A_1 increasing slowly from ~0.60 at 50 °C to ~0.80 at 250 °C, while A_1 for sample FL1 increases from ~0.40 to ~0.70 between 50 °C and 150 °C, and subsequently stays constant. Fig. 8b shows the corresponding background parameter *bgd* at the various stimulation temperatures. It is seen that for three of the samples this amplitude increases from a value of ~0.001 at 50 °C to a value of ~0.010 at 250 °C. The fourth sample FL1 shows a gradual decrease from ~0.010 to ~0.007, followed by an increase to ~0.015 at the highest stimulation temperature. It is hypothesized that this background signal contains contributions from three

sources: dark counts, isothermal signal, and possibly very slow relaxation processes. This contribution of this background to the overall TR-IRSL signal is discussed in detail in [13].

4. Discussion

4.1. "Fast" and "Slow" TR-IRSL signals—luminescence pathways in feldspars

In this section we discuss a possible interpretation of the results shown in Fig. 7, in terms of the experimental results and proposed model of Jain and Ankjærgaard [1]. Recent extensive experimental work by these authors has elucidated the complexity of the luminescence processes in feldspars. Their time-resolved experiments were carried out using both resonant excitation using IR LEDs, as well as non-resonant excitation with green and blue LED stimulation. These experiments showed that the use of stimulation light of different wavelengths allows the separation of resonant IR excitation and non-resonant blue/green excitation processes in feldspars. These authors examined the changes occurring in the TR-OSL decay shape as a function of photon energy, storage time after irradiation, and thermal or optical pre-treatments of the samples. Their results were interpreted within the framework of a model containing several possible recombination routes, namely (a) via the ground state and the excited state of the trap, (b) via the band tail states and (c) through the conduction band. Ground state tunneling is the most localized recombination process, while conduction band recombination processes are highly delocalized, and therefore are likely to access the entire crystal.

The IRSL trap in feldspar is believed to be located at ~2–2.5 eV below the conduction band, and therefore optical stimulation with blue light at a photon energy of 2.63 eV causes a direct transition into the conduction band. However, stimulation with IR light of a wavelength of ~1.4 eV causes resonant electronic transitions from the ground state into the excited state of the trap. Excitation with green LEDs causes electronic transitions of an intermediate nature, between blue and IR excitation energies. It is also believed that a continuum of thermal excitations can take place from the bottom edge of the band tail states, into the excited state of the trap, and eventually into the conduction band. Jain and Ankjærgaard [1] concluded that electrons from the excited state can either recombine with holes directly by tunneling, or they may be involved in band tail transport through the crystal.

The results of these and other recent experimental studies (Poolton et al. [21]; Thomsen et al. [24]) suggested that the luminescence production mechanism in feldspars depends critically on the distance between the electron and the hole traps in these materials. This distance seems to be one of the more important elements in determining the shape of luminescence signals from these materials. Recent modeling work by Pagonis et al. [25] also supports the important role played by this parameter in the production of continuous-wave IRSL (CW-IRSL) signals. These authors presented a model which explained the dependence of the shape of CW-IRSL signals on the power of the stimulating light, based on the experimental work of Thomsen et al. [24].

Jain and Ankjærgaard [1] interpreted changes taking place in the shape of their signals, on the basis of changes taking place on the average distance between donors and acceptors. These authors emphasized that the TR-OSL decay form cannot be interpreted simply as a linear sum of exponential decays. In order to analyze their data these authors defined two integral regions termed as the 'Fast signal' and the 'Slow signal'. The Fast signal was estimated by proxy, using the total integrated signal during the stimulation time (0–50 μs). The Slow signal was defined as the slowly decaying component obtained by integrating from 100 to 550 μs when the IR stimulation has been turned off. The form of the IR and green stimulated TR-OSL decay signals was strongly dependent on the stimulation photon energy, suggesting that these signals most likely arise from different electronic pathways. The difference between the initial decay rates of the IR and green stimulated Fast signals led the authors to suggest that the *IR Fast signal originates mostly from nearest-neighbor recombinations*, which take place from the excited state of the trap and the proximal band tail states. Furthermore, the authors also suggested that the *IR and green Slow signals originate from distant recombinations* taking place via a slower transport within the band tail states. This latter slower process is likely to be a combination of two competing processes, a phonon assisted diffusion and a tunneling process.

In the next section the results of Fig. 7 are discussed within this proposed model of luminescence processes in feldspar [1].

4.2. The effect of stimulation temperature on the initial decay rate of TR-IRSL signals

In this paper, TR-IRSL data is fitted with a linear combination of an exponential decay and a stretched exponential function. These two fitting functions are characterized by a rather short decay time τ_1, and a much larger decay time parameter τ_0 correspondingly. Furthermore, the SE function is associated with a continuous distribution of lifetimes and decay rates, examples of which were shown in Fig. 2. As with any semi-empirical approach, it is not possible to "prove" that the fitting function in Eq. (15) is the "correct one". However, in the following discussion it will be shown that the general conclusions from Ref. [1] are consistent with the results of Fig. 7 in this paper.

Jain and Ankjærgaard [1] concluded from their data analysis that IR stimulation causes an *increase* in the initial decay rate of the Fast signal with stimulation temperature, due to an increase in the recombination probability. Their TR-IRSL data showed a large increase in the decay rate with stimulation temperatures from 50 to 100 °C, and that thereafter the decay rate remained generally constant (Ref. [1], inset, Fig.4). The change in the decay rate of the IR Fast signal from 50 °C to 100 °C was interpreted as follows: at higher stimulating temperatures an increased proportion of electrons escapes from the excited state of the trap, and are raised into higher energy band tail states; these energy states are likely to allow relatively efficient sub conduction band edge transport. Band tails in feldspars are characterized by a variety of well depths, widths and separations (see for example the discussion in Poolton et al., [22]). In terms of the corresponding electron wave-function in these materials, one would expect this wave-function to be more extended in space at higher stimulation temperatures (Poolton et al., [21–23]), which would lead in turn to an increased probability of hopping. As a consequence, higher charge mobility would cause a quicker recombination process, which would be seen as an increase in the decay rates.

The exponential component data in Fig. 7a show that as the stimulation temperature increases, the characteristic decay time τ_1 decreases, consistent with the proposed model in [1]. In addition, the discussion in [1] pointed out that the model predicts a relatively small dependence of the Fast signal on the stimulation temperature. This is also consistent with the data in Fig. 7a, which shows that the decay time τ_1 for three of the studied samples varies by less than 10% over the range of stimulation temperatures. The behavior of sample FL1 was notably different, with time τ_1 decreasing by almost 50% over the range of stimulation temperatures.

By inspection of the data in Fig. 7a, one might expect that the exponential decay component in Eq. (15) will make a significant contribution to the TR-IRSL signal only within ~5 characteristic decay times, i.e. for the initial time period of $\sim 5\tau_1 \sim 10$ μs. This is also consistent with the description and interpretation of the "Fast signal" in Ref. [1].

It is noted that Jain and Ankjærgaard ([1], inset of their Fig. 4), observed a large change in the decay rate of their Fast signal between stimulation temperatures of 50 and 100 °C. Our data does not show the same large change in the decay rate, and this result should be investigated in future work in other types of feldspars.

4.3. The effect of stimulation temperature on the slower component of TR-IRSL signals

Within our interpretation scheme of the empirical Eq. (15), the main difference between the Fast and Slow TR-IRSL signals is that the former signal arises from a more *localized* recombination than the latter.

Jain and Ankjærgaard [1] pointed out that, since the IR energy matches the excited state energy of the trap, and the energy of the green light is close to the ionization energy, the Fast signal arising from these processes should show a rather small thermal dependence. As mentioned previously, this prediction is in agreement with the fitting results of Fig. 7a. However, these authors also point out that one might expect a greater thermal dependence for the Slow signal, which is hypothesized to arise from charge transport through the band tail states, due to the Phonon Assisted Diffusion (PAD) mechanism. This behavior was observed and quantified for the Slow signals in Ref. [1], with these signals indeed exhibiting a much larger activation energy of 0.14 eV for both the IR and green stimulations.

The SE data in Fig. 7b show that the characteristic time τ_0 of the SE component varies with the stimulation temperature T, with the four samples studied showing different behaviors. Fig. 7b shows that as T is increased, the decay time τ_0 characterizing the SE function for samples FL2_1 and FL2_2 gradually *decreases* from a value of ~10 μs at 50 °C, to a smaller value of ~8 μs at 250 °C. Samples FL1 and FL3 show a non-monotonic behavior, with the decay time τ_0 increasing for temperatures upto ~150 °C, followed by a gradual decrease at the higher stimulation temperatures.

The SE data in Fig. 7c show also a different behavior for parameter β in the four samples studied. The SE parameter β for samples FL2_1 and FL2_2 remains practically constant at $\beta \sim 0.80 + 0.01$ at the various stimulation temperatures. Sample FL1 shows a different behavior, namely a constant value of $\beta \sim 0.66$ upto a stimulation temperature of 100 °C, followed by a gradual decrease of this parameter to $\beta \sim 0.55$ at the higher stimulation temperatures. Sample FL3 also shows a different behavior, namely a small gradual increase from a value of $\beta \sim 0.40$ to a value of $\beta \sim 0.47$ at the higher stimulation temperatures.

These different behaviors of the four samples are most likely indicative of the presence of multiple slower competing processes, taking place at higher stimulation temperatures. It is hypothesized that these competing processes may involve both band tail states and/or the conduction band. According to the proposed band structure in Ref. [1] (their Fig. 3), there exists a continuum of thermal excitations from the bottom edge of the band tail states to the excited state of the trap and eventually to the conduction band. Electrons which are thermally evicted into the band tail states undergo localized recombination, the extent of which depends upon electron mobility. The higher the stimulation temperature, the higher the occupied energy level, and the more delocalized the recombination process.

Jain and Ankjærgaard [1] pointed out that in contrast to the Fast TR-IRSL signal, the rate of depletion of the Slow signal for their sample seemed to *decrease* at higher stimulation temperatures. They attributed this apparent decreased rate of depletion of the Slow signal to the presence of retrapping effects into the e–h trap. Such retrapping effects are likely to occur due to the spatial association of the evicted electrons to the parent trap. These authors also pointed out that these retrapping effects compete with an increased probability of hopping and a higher electron mobility, both of which are more prevalent at higher stimulation temperatures. The increased hopping and mobility of the charge carriers can be attributed to a more extended wave-function, combined with an exponential increase in the density of states at higher stimulation temperatures. These two effects (retrapping and increased hopping/mobility) would affect the decay rates in opposite directions at increasing stimulation temperatures. It is then possible that competition between these opposing processes leads to the complex behaviors shown in Fig. 7b and c.

Clearly, further experimental and modeling work is necessary to ascertain whether the behavior exhibited in Fig. 7 constitute a universal behavior of feldspar samples.

5. Conclusions

In this paper, a new method is suggested for analyzing TR-IRSL signals from feldspars. The new method was used successfully to fit complete sets of experimental data for four feldspar samples, and for stimulation temperatures between 50 °C and 250 °C.

The fitting in Eq. (15) is certainly empirical, and it is possible to fit this experimental data with other combinations of functions, and to achieve equally good, or even better fits to the data. As mentioned above, Fig. 5 shows an alternative excellent fit to the experimental data, using the linear combination of three exponential functions. However, recent experimental work on feldspars ([1,2]) supports the presence of several possible luminescence pathways in these materials, and has led to serious doubts concerning the validity of analyzing these signals using a linear combination of exponential functions.

We believe that the combination of functions used in this paper has the following advantages. Firstly, it has the advantage of requiring fewer fitting parameters than the 3-exponential fitting procedure; while Eq. (15) has five fitting parameters, the normalized linear combination of three exponentials requires six fitting parameters.

Secondly, the use of a stretched exponential to describe the TR-IRSL signals from feldspars has a possible physical basis, since it can be *tentatively* associated with physical processes underlying the mathematical expressions. Specifically, the use of the stretched exponential function is consistent with extensive theoretical work on hopping mechanisms in solids, as well as on tunneling processes [10,11]. Whether these functions also apply to feldspars is an open question in research. In addition, experimental work has provided direct experimental evidence for the existence of band tail states in feldspars, at least at low temperatures (Poolton et al. [21]).

Thirdly, the distributions $H(k)$ and $f(\tau)$ of time decay constants $k(t)$ and time constants $\tau(t)$ correspondingly, can be extracted from the stretched exponentials as shown in Fig. 2, since their mathematical properties have been studied previously rather extensively.

Finally, it has been previously suggested that one could use the SE functions on a complete empirical basis; in this case the stretched exponential fits to the experimental TR-IRSL data provide an indication of the amount of deviation of the luminescence decay law from an exponential behavior [12].

From the point of view of luminescence dating, a key component of the model in [1] is that the Slow TR-IRSL signal preferentially selects electrons that lack proximal donor–acceptors, and one would then expect it to be more stable thermally. This prediction was confirmed from the fading experiments in all the samples examined in [1]. The new method of analysis proposed in this paper can help isolate mathematically the more thermally stable components, and hence could lead to better dating applications in these materials.

Acknowledgments

We thank Dr. Christina Ankjærgaard and Dr. Mayank Jain for providing us with a digital copy of their experimental TR-IRSL data shown in Fig. 3, as well as for the additional sets of data not shown in this paper. Dr. Vasilis Pagonis is also grateful for the financial support of the National Laboratory for Sustainable Energy, in Roskilde, Denmark during his visit in October, 2010.

An anonymous referee is thanked for their extensive and constructive comments, which have led to a major revision and to a much improved version of this paper. We also thank Dr. A.J.J. Bos of Delft University for analyzing the data using the ORIGIN software package.

References

[1] M. Jain, C. Ankjærgaard, Radiat. Meas. 46 (2011) 292.
[2] C. Ankjærgaard, M. Jain, J. Phys. D: Appl. Phys. 43 (2010) 255502.
[3] D.C.W. Sanderson, R.J. Clark, Radiat. Meas. 23 (1994) 633.
[4] R.J. Clark, I.K. Bailiff, Radiat. Meas. 29 (1998) 553.
[5] R.J. Clark, I.K. Bailiff, M.J. Tooley, Radiat. Meas. 27 (1997) 211.
[6] M.L. Chithambo, R.B. Galloway, Meas. Sci. Technol. 11 (2000) 418.
[7] P.M. Denby, L. Bøtter-Jensen, A.S. Murray, K.J. Thomsen, P. Moska, Radiat. Meas. 41 (2006) 774.
[8] S. Tsukamoto, P.M. Denby, A.S. Murray, L. Bøtter-Jensen, Radiat. Meas. 41 (2006) 790.
[9] C. Ankjærgaard, M. Jain, R. Kalchgruber, T. Lapp, D. Klein, S.W.S. McKeever, A.S. Murray, P. Morthekai, Radiat. Meas. 44 (2009) 576.
[10] M.N. Berberan-Santos (Ed.), Fluorescence of Supermolecules, Polymers and Nanosystems, Springer, Berlin, 2008.
[11] R. Chen, J. Lumin. 102–103 (2003) 510.
[12] M.N. Berberan-Santos, E.N. Boduno, B. Valeur, Chem. Phys. 315 (2005) 171.
[13] P. Morthekai, J. Thomas, M.S. Padian, V. Balaram, A.K. Singhvi, Radiat. Meas., http://dx.doi.org/10.1016/j.radmeas.2012.03.007, in press.
[14] T. Lapp, M. Jain, C. Ankjærgaard, L. Pirzel, Radiat Meas. 44 (2009) 571.
[15] L. Bøtter-Jensen, K.J. Thomsen, M. Jain, Radiat. Meas. 45 (2010) 253.
[16] F. James, M. Roos, MINUIT, CERN program library entry D506. 〈http://consult.cern.ch/writeups/minuit〉, 1977.
[17] G. Adamiec, M. Garcia-Talavera, R.M. Bailey, P. Iniguez de la Torre, Geochronometria 23 (2004) 9.
[18] G. Adamiec, A. Bluszcz, R.M. Bailey, M. Garcia-Talavera, Radiat. Meas. 41 (2006) 897.
[19] A. Bluszcz, G. Adamiec, Radiat. Meas. 41 (2006) 886.
[20] H.G. Balian, N.W. Eddy, Nucl. Instrum. Methods 145 (1977) 389.
[21] N.R.J. Poolton, R.H. Kars, J. Wallinga, A.J.J. Bos, J. Phys.: Condens. Matter 21 (2009) 485505.
[22] N.R.J. Poolton, J. Wallinga, A.S. Murray, E. Bulur, L. Bøtter-Jensen, Phys. Chem. Miner. 29 (2002) 210.
[23] N.R.J. Poolton, K.B. Ozanyan, J. Wallinga, A.S. Murray, L. Bøtter-Jensen, Phys. Chem. Miner. 29 (2002) 217.
[24] K.J. Thomsen, A.S. Murray, M. Jain, Geochronometria 38 (2011) 1, http://dx.doi.org/10.2478/s13386-011-0003-z.
[25] V. Pagonis, M. Jain, A.S. Murray, C. Ankjærgaard, R. Chen, Radiat. Meas., http://dx.doi.org/10.1016/j.radmeas.2012.02.012, in press.